Wiley
International Journal of Energy Research
Volume 2024, Article ID 8984734, 11 pages
https://doi.org/10.1155/2024/8984734

WILEY

Research Article

Improved CO Selectivity via Anion Exchange Membrane Electrode Assembly-Type CO_2 Electrolysis with an Ionomer-Coated Zn-Based Cathode

Junhyeong Kim,[1] Gyeong Ho Han,[1] Jung Yong Seo,[2] Minji Kang,[2] Myung-gi Seo,[2] Youngheon Choi,[2] Soo Young Kim,[3] and Sang Hyun Ahn[1]

[1]*Department of Chemical Engineering, Chung-Ang University, Seoul 06974, Republic of Korea*
[2]*Lotte Chemical Institute of Technology, Daejeon 34110, Republic of Korea*
[3]*Department of Materials Science and Engineering, Korea University, Seoul 02841, Republic of Korea*

Correspondence should be addressed to Soo Young Kim; sooyoungkim@korea.ac.kr and Sang Hyun Ahn; shahn@cau.ac.kr

Received 26 March 2024; Revised 16 May 2024; Accepted 21 May 2024

Academic Editor: Ahmad Azmin Mohamad

Zn is a promising electrocatalyst candidate for CO production via CO_2 electrolysis because of the moderate binding energy of *COOH intermediate. However, its thermodynamically unstable properties could cause performance degradation, particularly in conventional H-type electrolysis systems where the electrocatalyst is directly in contact with the electrolyte. Herein, we investigate the unstable characteristics of Zn-based cathode and suggest employing the anion exchange membrane electrode assembly- (AEMEA-) type CO_2 electrolysis system to mitigate the electrolyte effects and enhance the catalytic performance. Unlike the conventional H-type electrolyzer, an AEMEA-type electrolyzer with a zero-gap configuration could mitigate the electrolyte effects on the cathode, thereby suppressing surface oxidation of the Zn-based cathode during the electrochemical reaction. Furthermore, the anion exchange ionomer layer on the cathode provides numerous ion pathways between catalyst and membrane interfaces and increases catalyst utilization that enhances the activity and selectivity for CO production via CO_2 electrolysis. The above results suggest the breakthrough of using unstable materials as a catalyst for CO_2 electrolysis and achieving reasonable performance.

1. Introduction

CO_2 electrolysis, which electrochemically converts CO_2 into various hydrocarbon fuels, has the potential to reduce the dependence on fossil fuels and restrain the acceleration of global warming [1–4]. Among the products obtained via CO_2 electrolysis, CO presents advantages in commercial utilization owing to its market price and wide range of applications [5–9]. Many studies have reported that Zn, which exhibits reasonable performance for CO production with high selectivity [10–14], has considerable interest as an alternative to noble metals such as Au and Ag [15–20]. However, Zn has a low standard reduction potential (E°: $-0.76\,V_{NHE}$), and it is easy to chemically oxidize to hydroxide where the Zn is used as an electrode in conventional H-type electrolyzer [21]. Moreover, the thermodynamically unstable Zn dissolves into the electrolyte, which becomes more serious under acidic conditions. These corrosion phenomena could lead to stability issues during the CO_2 electrolysis with a Zn-based catalyst [22]. Thus, minimizing the direct contact between the catalyst surface and the electrolyte is necessary.

Meanwhile, CO_2 electrolysis using a gas diffusion electrode is attracting attention because it can overcome the mass transfer issues by directly supplying gaseous CO_2 onto the catalyst surface, thereby achieving hundreds of milliamperes per square centimeter for the desired reactions [23–25]. Among the gas-phase CO_2 electrolysis systems, a membrane electrode assembly- (MEA-) based system consists of a cathode, anode, and polymer membrane located between two electrodes with zero gap [23, 26–28]. Because

of MEA configuration with zero-gap design, no catholyte layer is required, thereby improving the energy efficiency of the system and mitigating direct contact between catalyst and electrolyte [29].

In particular, the anion exchange membrane (AEM) provides an alkaline atmosphere near the cathode suitable for CO_2 electrolysis, resulting in the fact that the AEM-based MEA- (AEMEA-) type electrolyzer system exhibits higher product selectivity than the proton exchange membrane- (PEM-) based MEA- (PEMEA-) type one [30, 31]. Furthermore, many studies for combining the anion exchange ionomer (AEI) onto the cathode have been conducted to further improve the performance via CO_2 electrolysis [32–34]. Kim et al. confirmed that the AEI layer contributed to increasing the local CO_2/H_2O ratio because the AEI can impede the cation transport owing to Donnan exclusion [32, 35]. Patru et al. also investigated the influence of an alkaline environment near the cathode onto CO_2 electrolysis [33]. In addition, the application of AEI, which has the advantages of providing ion pathway between catalyst and membrane interfaces and increasing catalyst utilization, could exhibit the improved CO_2 electrolysis performance and stability [36].

Herein, we demonstrated the necessity of an AEMEA-type CO_2 electrolysis system when using an unstable Zn-based electrocatalyst. First, we investigated the unstable properties of Zn-based catalyst under an aqueous electrolyte occurring morphological and chemical change. It was confirmed that employing the AEMEA-type electrolyzer system could well preserve the Zn-based catalyst during the CO_2 electrolysis and enhance the activity with high CO selectivity. Moreover, the AEI layer onto the cathode provided the local alkaline environment and improved the performance of CO production via AEMEA-type CO_2 electrolysis.

2. Experimental

2.1. Electrodeposition of Zn-Based Catalyst. The Zn-based catalyst for the CO_2 electrolysis was fabricated by a facile electrodeposition method. A home-made Teflon cell with 1.44 cm^2 of exposed area was used as the three-electrode cell system and was connected with a potentiostat (Autolab, PGSTAT302N, Metrohm). The working electrode had a microporous layer on a carbon paper (MPL/CP). A saturated calomel electrode (SCE) and a Pt wire were used as the reference and counter electrodes, respectively.

Prior to the electrodeposition, the MPL/CP surface was electrochemically pretreated at 5 mA/cm^2 for 100 s in a 0.5 M $(NH_4)_2SO_4$ solution to improve the surface hydrophilicity. The deposition electrolyte was composed of 0.2 M $ZnSO_4{\cdot}7H_2O$, 0.5 M $(NH_4)_2SO_4$, and 1.0 M H_2SO_4. The electrodeposition for the Zn/MPL/CP fabrication was conducted by applying a constant potential at −2.1 V_{SCE} until the deposited charge amount was leached at −50 C. The deposition solution was N_2-purged before the electrodeposition step to remove the dissolved O_2 species.

2.2. Ionomer Coating on As-Prepared Zn/MPL/CP. The ionomer was spray coated on the as-prepared Zn/MPL/CP to further improve the CO_2 electrolysis performance. The ionomer solution consisted of 736 μL of deionized water (DI), 64 μL of the ionomer (XA-9, Dioxide Materials), and 3.2 mL of isopropyl alcohol (IPA). The ionomer-coated Zn/MPL/CP cathode was dried at 50°C for 30 min to evaporate the residual IPA.

2.3. Characterization. Field-emission scanning electron microscopy (FESEM, Sigma, Carl Zeiss) and energy-dispersive X-ray spectroscopy (EDS, Thermo, NORAN System 7) analyses were conducted to investigate the surface morphology and bulk atomic composition of the as-prepared Zn/MPL/CP. The bulk crystal structure was also observed through X-ray diffraction (XRD, Bruker, D8 Advance). The electronic structure and surface composition were analyzed by X-ray photoelectron spectroscopy (XPS, K-alpha+, Thermo Fisher Scientific). In addition, the Raman (LabRAM HR Evolution, HORIBA) analysis was conducted to confirm the oxidation state of the Zn/MPL/CP surface.

2.4. Electrochemical Measurements in the Conventional H-Type Electrolysis System. The CO_2 electrolysis performance in an H-type cell system was verified for 20 min at each constant potential. The as-prepared Zn/MPL/CP was used as the working electrode in an H-type electrolyzer. Further, Pt-mesh and SCE were used as the counter electrode and reference electrode, respectively. The working and counter electrodes were separated by a membrane, and Nafion 212 (Dupont Co.) and Sustainion X37-50 (Dioxide Materials) were used for the proton exchange membrane- (PEM-) based H-type electrolyzer and AEM-based H-type electrolyzer, respectively. The active area for electrodeposition was 1.0 cm^2.

The CO_2-purged and N_2-purged 0.5 M $KHCO_3$ electrolytes were contained in the cathode and anode, respectively. Then, the CO_2 was continuously injected with a flow rate of 10 mL/min by modulating the mass flow controller (MKS Instruments, Inc.). The measured potential was converted to a reversible hydrogen electrode (RHE) with the following formula: $E_{RHE} = E_{SCE} + 0.2412 + 0.0592 \times pH$. The outlet of each electrolyzer was connected to a gas chromatograph (GC, Agilent 7890B) to measure the concentrations of the gas products (H_2 and CO).

The gas products from the electrolyzer were gained for 1 min before the end of each potential measurement, and simultaneously, the flow rate of the outlet was detected by the mass flow meter. The Faradaic efficiency (FE) for each product was calculated by integrating the concentration from GC, flow rate, and the charge amount during the time of product gained. The partial current density (PCD) which represents the current density for a specific product obtained was calculated by multiplying the total current density with FE.

2.5. Electrochemical Measurements in the MEA-Type Electrolysis System. Unlike the conventional H-type cell system, the MEA-type electrolyzer was connected with a two-electrode cell system. The Zn/MPL/CP was used as the cathode, and the commercial IrO_2/CP (C0206 Dioxide

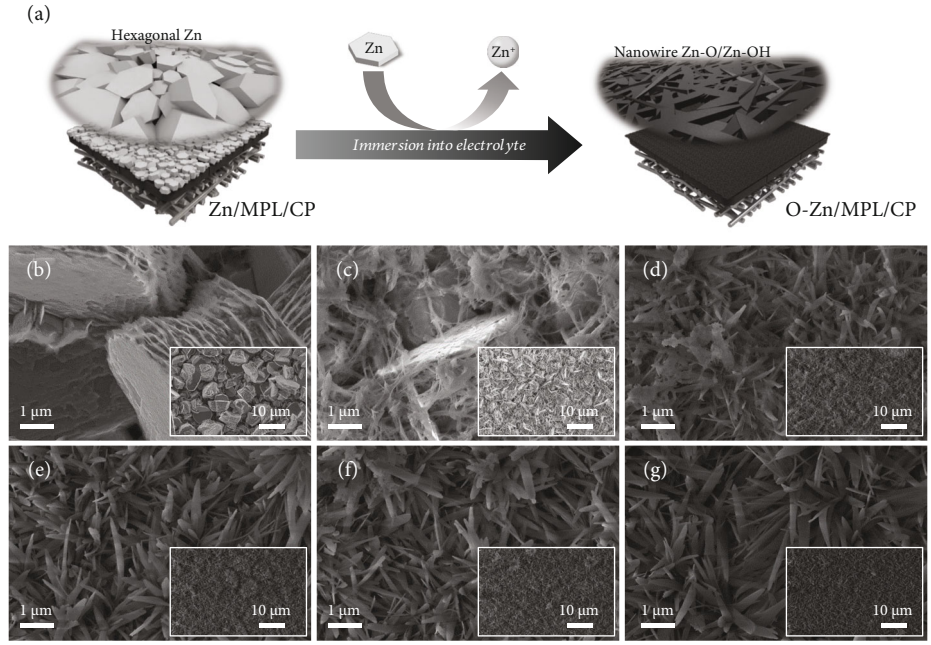

FIGURE 1: (a) Schematic image of the morphological transformation of the hexagonal Zn-based catalyst. High- and low-magnification (inset) FESEM images of the Zn/MPL/CP after immersion into 0.5 M $KHCO_3$ for varying times: (b) 0 min (bare Zn/MPL/CP), (c) 5 min, (d) 20 min, (e) 40 min, (f) 60 min, and (g) 180 min.

Materials) was used as the anode. In the case of the MEA-type electrolyzer, the membrane (PEM: Nafion 212, Dufont Co., AEM: sustainion x37-50, Dioxide Materials) was located between the cathode and anode with a zero-gap configuration, where the active area was 1.0 cm^2.

Humidified CO_2 gas was supplied into the backside of the Zn/MPL/CP cathode with a flow rate of 200 mL/min. On the anode side, DI and 0.1 M KOH were injected with a flow rate of 20 mL/min for the PEMEA and AEMEA-type electrolyzers, respectively. The FE and PCD for CO and H_2 from the MEA-based electrolyzer were calculated in the same manner as the H-type electrolyzer.

3. Results and Discussion

3.1. Characterization of the Instability of the Zn-Based Catalyst. Prior to testing the CO_2 electrolysis performance, we investigated the unstable properties of the Zn-based catalyst under an aqueous electrolyte. The Zn/MPL/CP was fabricated by electrodeposition on the MPL/CP substrate (Figure S1), and the FESEM image shows that the Zn deposits with the hexagonal structure were well distributed (Figure 1(b)). However, when the as-prepared Zn/MPL/CP was immersed into a 0.5 M $KHCO_3$ electrolyte, the hexagonal structure gradually changed to a dendrite (Figure 1). This morphological change in the Zn-based catalyst was due to the difference in the dissolution rates based on the crystal structures, which was confirmed in our previous study [37]. The conversion to the dendrite structure was saturated at an immersion time of 180 min, which indicates the unstable properties of the Zn materials in the electrolytes.

Figure 2 shows the comparison of the properties of the Zn/MPL/CP before and after immersion into the $KHCO_3$ electrolyte. The structural change in the Zn/MPL/CP was investigated by XRD analysis (Figure 2(a)). For the as-prepared Zn/MPL/CP, three peaks were detected in the XRD pattern (JCPDS #87-0713): Zn(002) at 36.3°, Zn(100) at 39.0°, and Zn(101) at 43.2°, indicating that the as-prepared Zn catalyst was close to the metallic state. In addition, the Zn(101) facet was dominant in the as-prepared Zn/MPL/CP, indicating that it was suitable for CO production via CO_2 electrolysis [13, 38]. After immersion into the 0.5 M $KHCO_3$ solution for 180 min, the new peak appeared at 31.8°, corresponding to the ZnO(100) facet.

As shown in Figure 2(b), compared to the Zn/MPL/CP, the ZnO(100)/Zn(100) intensity ratio increased in the I180-Zn/MPL/CP where the immersed time was 180 min. The additional results of the XRD patterns of the Zn/MPL/CP with varying immersion times are presented in Figure S2a and b. The XRD analysis revealed that a direct contact between Zn and the electrolyte caused not only a morphological change but also a chemical change from a metallic to an oxidized state.

Ex situ Raman spectroscopy was conducted to investigate the change in the surface structure of the Zn/MPL/CP after immersion for 180 min. As shown in Figure 2(c), two peaks at 387 cm^{-1} and 560 cm^{-1} were observed, which correspond to the characteristic vibrational mode of ZnO [12, 39]. In the case of the I180-Zn/MPL/CP, an increase in the peak intensity was observed at 387 cm^{-1}, 560 cm^{-1}, and ~240 cm^{-1}, which revealed that these are ascribed to the characteristic vibrational mode of $Zn(OH)_2$ [40].

Further, we demonstrated the electronic structures of the surfaces of the Zn/MPL/CP and I180-Zn/MPL/CP using the XPS analysis. As shown in Figure 2(d), the XPS spectrum of the Zn $2p_{3/2}$ region was deconvoluted into three peaks:

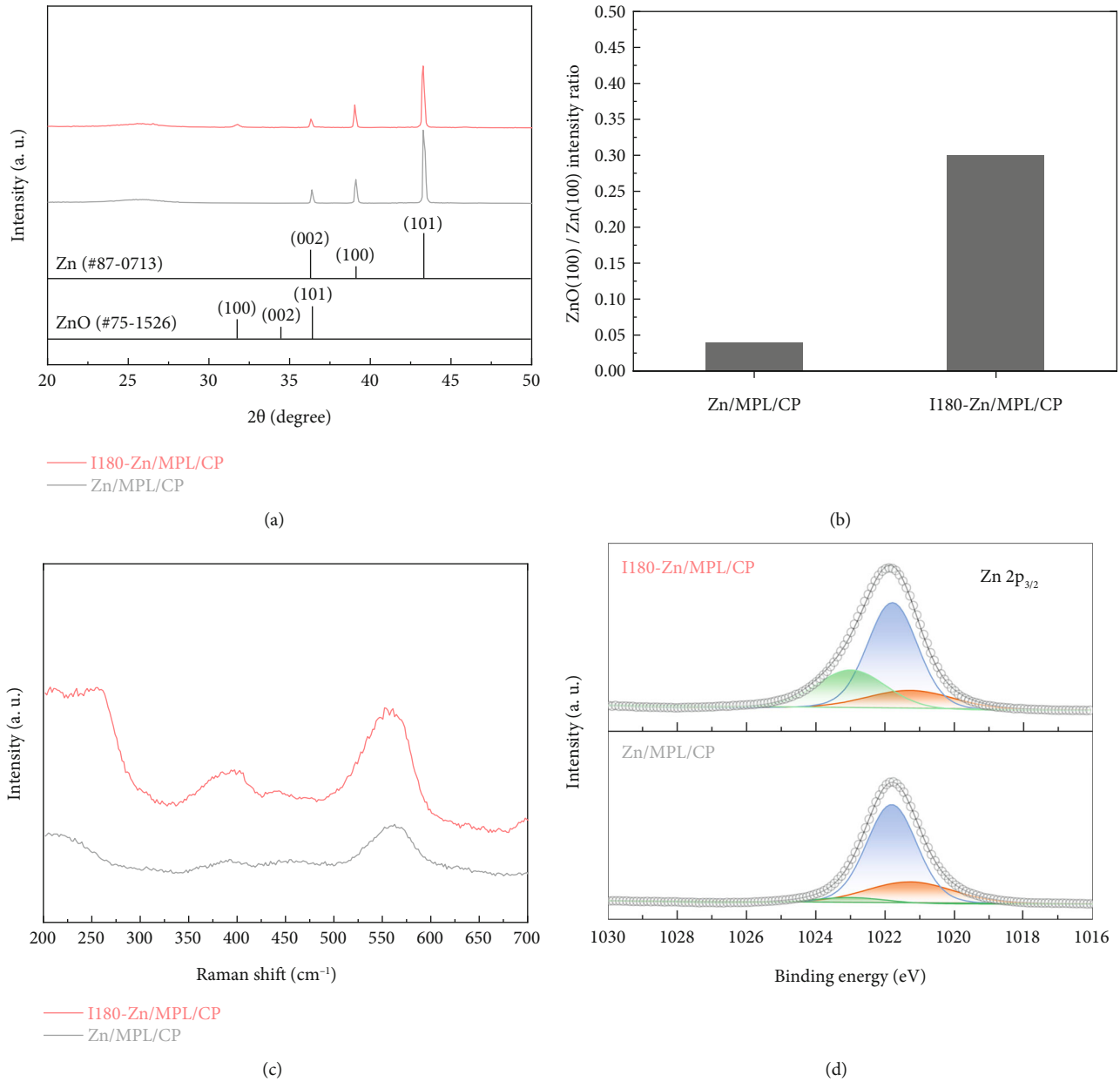

Figure 2: Continued.

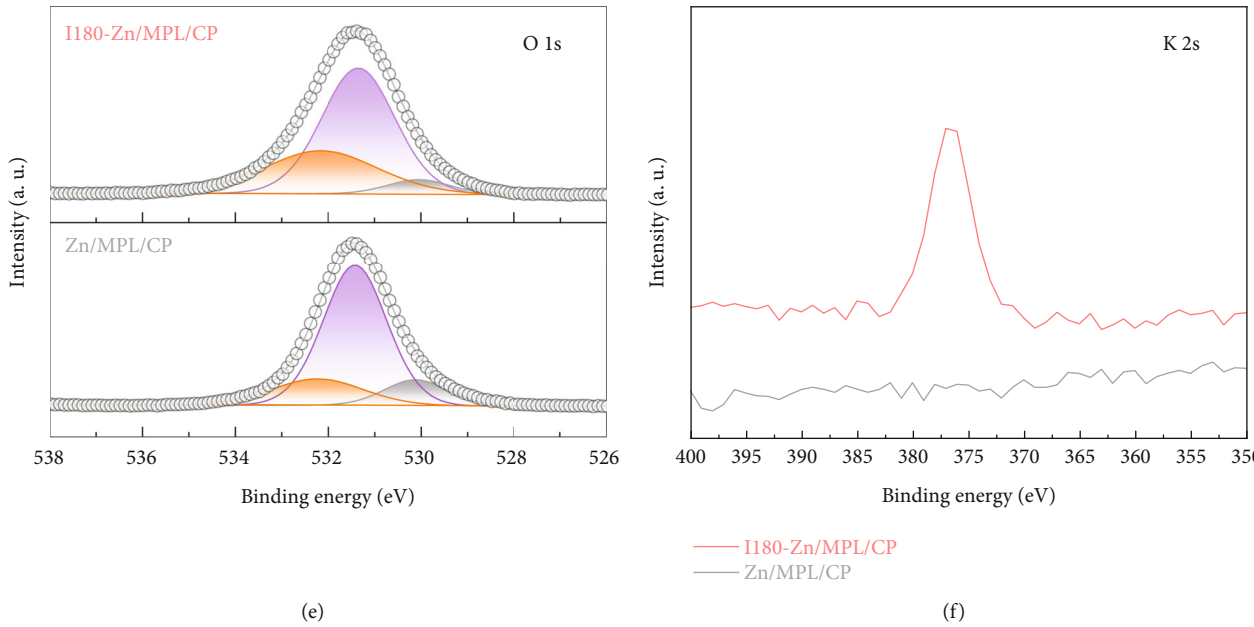

Figure 2: (a) XRD patterns of the as-prepared Zn/MPL/CP and I180-Zn/MPL/CP. (b) ZnO(100)/Zn(100) intensity ratio of the as-prepared Zn/MPL/CP and I180-Zn/MPL/CP corresponding to the XRD patterns. (c) Raman spectrum of the as-prepared Zn/MPL/CP and I180-Zn/MPL/CP. XPS spectra of the as-prepared Zn/MPL/CP and I180-Zn/MPL/CP: (d) Zn $2p_{3/2}$, (e) O 1 s, and (f) K 2 s.

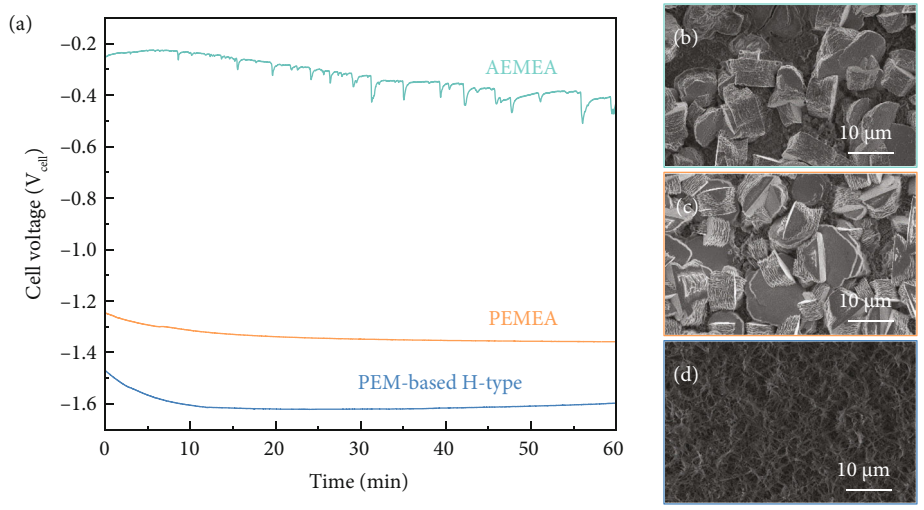

Figure 3: (a) Cell voltage variation during the open-circuit period according to the electrolyzer configurations (measured time: 60 min). FESEM images of the Zn/MPL/CP after the measurement: (b) AEMEA-type electrolyzer, (c) PEMEA-type electrolyzer, and (d) PEM-based H-type electrolyzer.

1021.3 eV, 1021.8 eV, and 1023.0 eV, which were assigned to metallic Zn, Zn-O, and Zn-OH, respectively [41]. After the immersion into the 0.5 M $KHCO_3$, the intensity of the metallic Zn was reduced, whereas those of the Zn-O and Zn-OH states increased. Meanwhile, three separated peaks were observed at O 1 s: 530.1 eV, 531.4 eV, and 532.2 eV, which were assigned to Zn-O, Zn-OH, and absorbed water molecules, respectively (Figure 2(e)) [41]. It was revealed that the ratio of Zn-OH and water molecules in the O 1 s peak increased after the immersion.

In addition, a significantly higher intensity at 376.6 eV representing the K 2 s state was observed in the I180-Zn/MPL/CP, which could be due to potassium incorporation into the surface (Figure 2(f)). The increase in the atomic compositions for O and K with the increasing immersion time was also confirmed by the EDS analysis (Figure S2c). The above results demonstrate that a direct contact between unstable Zn material and electrolyte causes surface oxidation and morphological changes.

3.2. Electrochemical Properties of the Zn/MPL/CP according to the Electrolyzer Type. Although various studies have reported on the high performance of the Zn-based catalysts in CO_2 electrolysis, the stability issues of the electrocatalysts

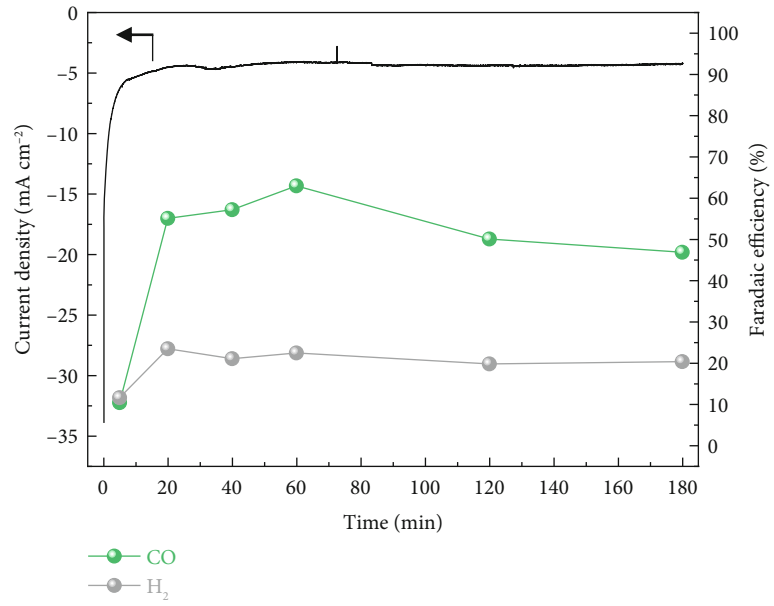

(a)

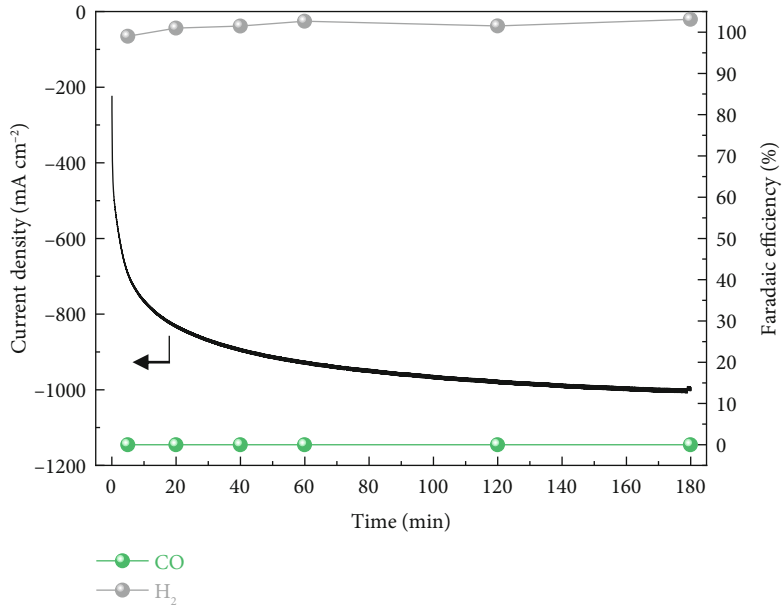

(b)

Figure 4: Continued.

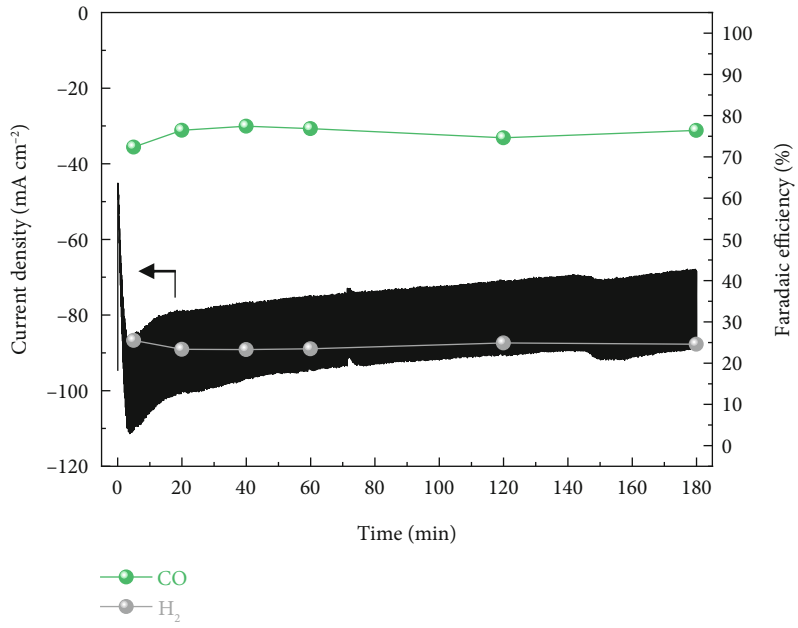

(c)

FIGURE 4: Total current density and FE for CO and H_2 production via CO_2 electrolysis for 180 min according to the electrolyzer configurations: (a) PEM-based H-type electrolyzer at −1.0 V_{RHE}, (b) PEMEA-type electrolyzer at −2.8 V_{cell}, and (c) AEMEA-type electrolyzer at −2.8 V_{cell}.

still remain unaddressed [11, 42]. In the conventional H-type cell for the CO_2 electrolysis, a direct contact between the electrode and electrolyte is inevitable, leading to performance degradation. To investigate the corrosion resistance of the Zn/MPL/CP as a cathode according to the electrolyzer configuration, the cell voltage variation in the two-electrode cell system was measured during the open-circuit period (Figure 3 and Figure S3).

In the conventional PEM-based H-type electrolyzer system, the measured cell voltage was started at −1.47 V_{cell}; however, the value decreased dramatically to −1.6 V_{cell} over 10 min and was then saturated (Figure 3(a)). Furthermore, the hexagonal structure of the Zn/MPL/CP was agglomerated and transformed into a dendrite after the measurement (Figure 3(d)), which corresponds to the FESEM images in Figure 1.

On the other hand, in the case of the PEMEA-type electrolyzer, a smooth decrease in the cell voltage from −1.25 V_{cell} to −1.36 V_{cell} within 60 min was observed. The hexagonal Zn structure was well preserved after the test, although there were weak surface damages (Figure 3(c)). Similar trends were also observed in the AEMEA-type electrolyzer, as shown in Figure 3(b). The EDS analysis after the measurement revealed that the metallic Zn state of the Zn/MPL/CP was well maintained when using the MEA-type electrolyzer (Figure S4). It means that the presence of a polymer membrane can mitigate the chemical oxidation of the Zn-based catalyst surface [43]. However, it should be noted that the precise comparison of the cell voltage variation was difficult because the ion migration differed according to the membrane and electrolyte used. Nevertheless, it implies that using MEA-type electrolyzer is essential not only for enhancing the CO_2 electrolysis performance but also for achieving durability.

3.3. Measurement of CO_2 Electrolysis Performance according to the Electrolyzer Type. We investigated the CO_2 electrolysis performance for 180 min at a constant potential according to the electrolyzer used (Figure 4). In the case of the PEM-based H-type electrolyzer, the Zn/MPL/CP cathode exhibited relatively low activity for the CO production at −1.0 V_{RHE} due to the poor solubility of CO_2 into the aqueous electrolyte (Figure 4(a)). Furthermore, the highest FE for the CO production was measured as 63% at 60 min, which steadily deteriorated with the increasing operation time. In addition to low CO_2 solubility, the ohmic loss owing to the presence of an electrolyte layer contributed to low CO_2 electrolysis performance.

In the case of PEMEA-type electrolyzer, hundreds of total current densities at −2.8 V_{cell} were obtained and gradually increased during the reaction (Figure 4(b)). It was because of the MEA configuration leading to improve energy efficiency and facilitate the mass transport. However, the calculated FE confirmed the most of the current density contributed to the hydrogen evolution reaction (HER) which is competing reaction against electrochemical CO_2 reduction. It was that the H^+ generated via the oxygen evolution reaction at the anode was transferred to the cathode through the PEM. As a result, the H^+ local concentration near the cathode surface was relatively higher than that of the CO_2 reactant.

On the other hand, the current density for CO production via CO_2 electrolysis was further enhanced in the AEMEA-type electrolyzer (Figure 4(c)). This indicated that

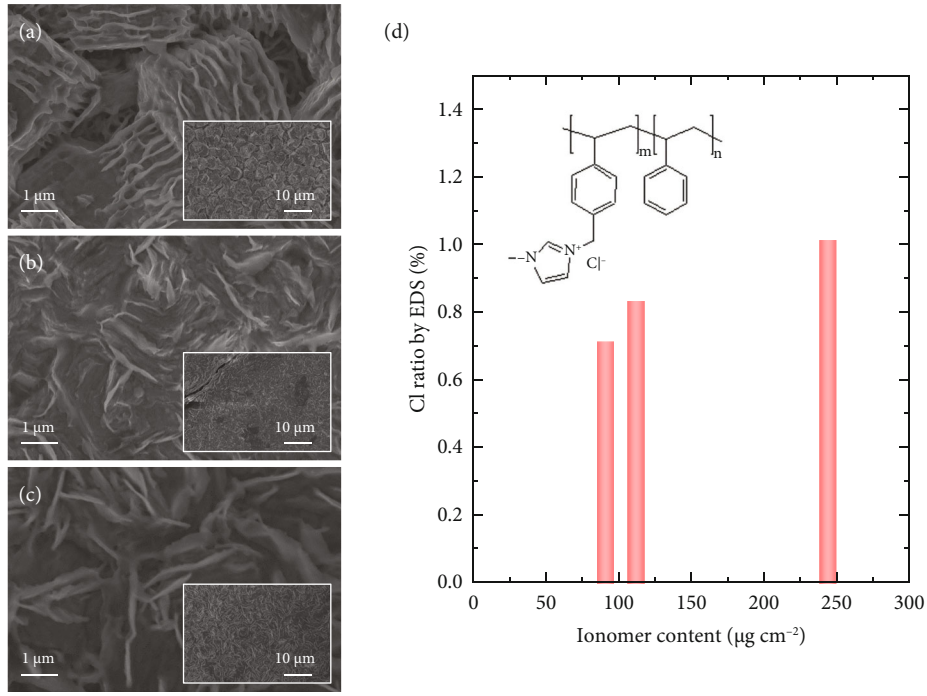

FIGURE 5: FESEM images of the AEI-coated Zn/MPL/CP cathode with varying amounts of AEI contents: (a) 90.2 μg/cm^2, (b) 111.1 μg/cm^2, and (c) 243.1 μg/cm^2. (d) Cl ratio in the AEI-coated Zn/MPL/CP cathode according to the ionomer content by EDS analysis (inset: structure of Sustainion XA-9 ionomer).

the AEM could suppress the accumulation of H^+ near the cathode mitigating the HER [44, 45]. Accordingly, the CO_2 electrolysis was dominant at the cathode and the AEMEA-type electrolyzer exhibited ~76% of stable CO FE for 180 min. Although there was slight performance degradation during the 180-min operation, the CO FE was well maintained, implying that the catalytic properties were unchanged.

The surface morphology of the Zn/MPL/CP cathode after the CO_2 electrolysis according to electrolyzer configuration was investigated by FESEM, which indicated that the Zn electrocatalysts were agglomerated with deformation in an PEM-based H-type system (Figure S5a). On the other hand, a damaged hexagonal surface was observed in the PEMEA-type electrolyzer due to the high H^+ concentration near the surface (Figure S5b).

In the case of the AEMEA-type electrolyzer, the hexagonal fixture of the Zn/MPL/CP was well maintained after 180 min of CO_2 electrolysis (Figure S5c). Furthermore, the AEMEA-type system exhibits the higher CO selectivity with high PCD at various applied potentials than other systems (Figure S6). This indicates that not only the MEA configuration, particularly when using AEM, but also the direct supply of gaseous CO_2 could provide reasonable CO_2 electrolysis performance while preserving the catalyst properties. The low K atomic ratio observed by the EDS analysis after the CO_2 electrolysis also indicated that the contribution of the catholyte in the AEM-based electrolyzer was reduced (Figure S5d).

3.4. Ionomer Effects on the AEMEA-Type CO_2 Electrolysis. To further enhance the CO_2 electrolysis performance, we introduced AEI layer on the top surface of the Zn/MPL/CP by spray-coating. The AEI layer provides an ion pathway and improves the interface properties between the electrode and membrane that can maximize the reaction active sites. The amount of AEI content was controlled by repeating the spray-coating process.

Figures 5(a), 5(b), and 5(c) show the FESEM images of the ionomer-coated Zn/MPL/CP cathode according to deposited AEI amounts. Compared to the as-prepared Zn/MPL/CP cathode (Figure 1(b)), the thin film was formed on the surface of the Zn/MPL/CP cathode containing 90.2 μg/cm^2 of the AEI, and the hexagonal structure was well preserved (Figure 5(a)). As the AEI content increased to 111.1 μg/cm^2, the hexagonal Zn interconnected with each other (Figure 5(b)), and an excessive amount of AEI (234.1 μg/cm^2) blocked the CO_2 gas passage (Figure 5(c)). Meanwhile, the EDS analysis indicated that with the increasing amount of AEI content, which consisted of chloride form, the Cl ratio increased (Figure 5(d)) [45].

The AEMEA-type CO_2 electrolysis performance for the AEI-coated Zn/MPL/CP cathodes was measured at –2.8 V_{cell} for 20 min (Figure 6). The CO FE exhibited an increasing tendency with the increasing amount of AEI, as shown in Figure 6(a). Correspondingly, the CO PCD improved from –68.1 mA/cm^2 to –107.8 mA/cm^2 (Figure 6(a)). However, the excessive amount of AEI coating (234.1 μg/cm^2) led to degradation of the CO PCD to –92.8 mA/cm^2 because of blockage in the pore structure and reduced active sites, as shown in Figure 5(c).

Meanwhile, the H_2 FE and H_2 PCD decreased after the AEI coating on the Zn/MPL/CP surface. It could be that the ionomer thin layer mitigates the accumulation of H^+ and allows the enhancement of CO selectivity. In addition,

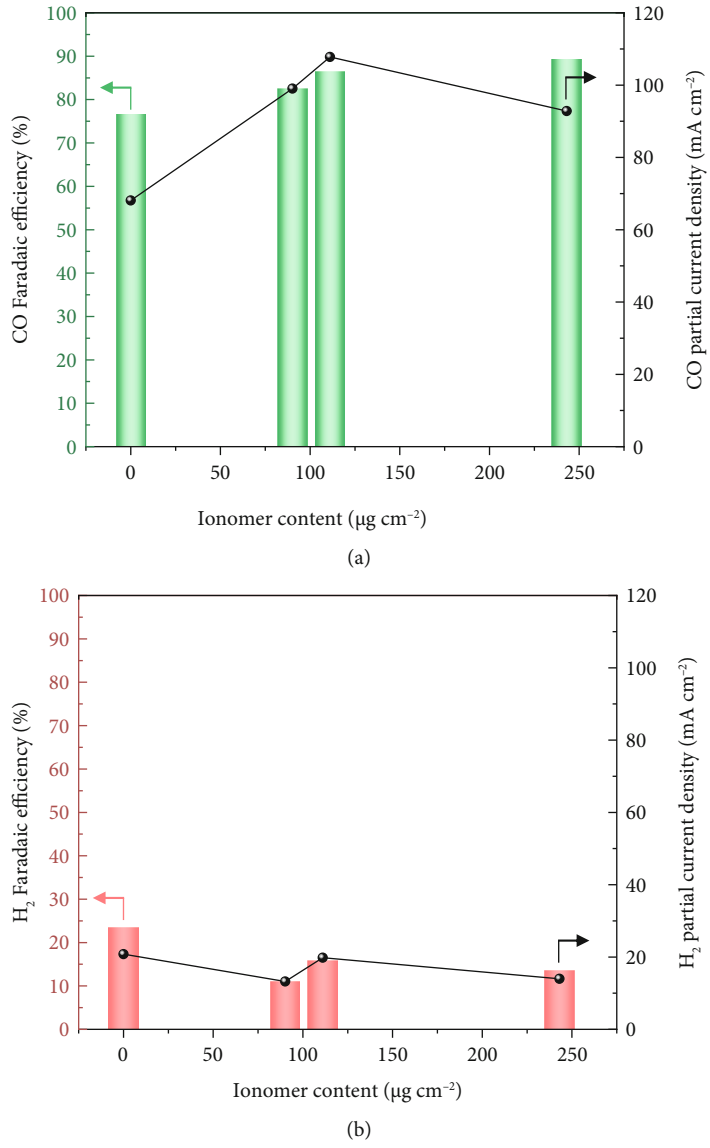

FIGURE 6: FE and PCD for (a) CO and (b) H_2 production via the AEMEA CO_2 electrolysis system with the Zn/MPL/CP cathode with varying AEI contents. Each electrolysis was conducted at −2.8 V_{cell} for 20 min (bar: FE; scatter + line: PCD).

during the AEMEA-type CO_2 electrolysis at −2.8 V_{cell} for 180 min, the AEI-coated Zn/MPL/CP cathode exhibited higher CO FE and CO PCD than those of the bare Zn/MPL/CP cathode. The additional electrochemical performance of AEI-coated Zn/MPL/CP according to the operating time is shown in Figure S7.

Moreover, the FESEM images in Figure S8 confirmed the hexagonal structure of the Zn/MPL/CP with the AEI content was well preserved after the CO_2 electrolysis for 180 min. This implied that the AEI thin layer could mitigate the access of the electrolyte or cations from the anode to the cathode, thus contributing to HER suppression. Additionally, the stability test for 12 h was conducted, and although there was a slight degradation in current density, the CO FE was well maintained at ~75% (Figure S9). It should be noted that we focused on systemic approaches for enhancing the performance and stability of CO_2 electrolysis with unstable Zn-based materials in this study; therefore, further development of a state-or-the-art electrocatalyst or an electrode with high performance is necessary to improve the overall system efficiency.

4. Conclusions

In this study, the unstable properties of Zn-based electrocatalysts were demonstrated in conventional H-type electrolyzer system, and, as a countermeasure, we suggested the importance of employing the AEMEA-type CO_2 electrolysis system to achieve a reasonable performance. The MEA configuration of AEMEA-type CO_2 electrolysis system mitigated the electrolyte effects onto the cathode resulting in well preserved hexagonal structure of as-prepared Zn catalyst after CO_2 electrolysis. In addition, the direct supply of gaseous CO_2 as well as employing the AEM contributed to obtaining

the stable performance for CO production. Furthermore, compared to the as-prepared sample, the AEI coating onto the cathode surface provided an ion pathway between catalyst and membrane interfaces, thereby exhibiting an enhanced CO FE from 77% to 89% and CO PCD from 68.1 mA/cm^2 to 107.8 mA/cm^2. Consequently, the above results have offered insights to achieve reasonable performance from CO_2 electrolysis with thermodynamically unstable catalyst.

Data Availability

Data is available on request.

Conflicts of Interest

There are no conflicts to declare.

Authors' Contributions

Junhyeong Kim and Gyeong Ho Han contributed equally to this work.

Acknowledgments

This research was supported by the National Research Foundation of Korea (NRF) grant funded by the Korean government MSIT (2021R1A2C2093358) and by the Chung-Ang University Graduate Research Scholarship in 2018. The authors also appreciate the financial support from LOTTE Chemical.

Supplementary Materials

Figure S1: FESEM image of MPL/CP substrate. Figure S2: XRD and EDS data of Zn/MPL/CP and I#-Zn/MPL/CP. Figure S3: schematic illustration of the electrolyzer configurations. Figure S4: bulk atomic composition of Zn/MPL/CP. Figure S5: FESEM images and K contents of Zn/MPL/CP after CO_2 electrolysis. Figure S6: performance of the Zn/MPL/CP in various CO_2 electrolyzer configurations. Figure S7: performance of the Zn/MPL/CP in AEMEA-type CO_2 electrolysis depending on the amount of ionomer content. Figure S8: FESEM images of Zn/MPL/CP after AEMEA-type CO_2 electrolysis. Figure S9: stability test of Zn/MPL/CP in AEMEA-type CO_2 electrolysis. *(Supplementary Materials)*

References

[1] C. Costentin, M. Robert, and J. M. Savéant, "Catalysis of the electrochemical reduction of carbon dioxide," *Chemical Society Reviews*, vol. 42, no. 6, pp. 2423–2436, 2013.

[2] K. P. Kuhl, E. R. Cave, D. N. Abram, and T. F. Jaramillo, "New insights into the electrochemical reduction of carbon dioxide on metallic copper surfaces," *Energy & Environmental Science*, vol. 5, no. 5, pp. 7050–7059, 2012.

[3] J.-P. Jones, G. K. S. Prakash, and G. A. Olah, "Electrochemical CO_2 reduction: recent advances and current trends," *Israel Journal of Chemistry*, vol. 54, no. 10, pp. 1451–1466, 2014.

[4] M.-Y. Lee, K. T. Park, W. Lee, H. Lim, Y. Kwon, and S. Kang, "Current achievements and the future direction of electrochemical CO_2 reduction: a short review," *Critical Reviews in Environmental Science and Technology*, vol. 50, no. 8, pp. 769–815, 2020.

[5] Y. Hori, K. Kikuchi, and S. Suzuki, "Production of CO and CH_4 in electrochemical reduction of CO_2 at metal electrodes in aqueous hydrogencarbonate solution," *Chemistry Letters*, vol. 14, no. 11, pp. 1695–1698, 1985.

[6] H.-R. M. Jhong, S. Ma, and P. J. A. Kenis, "Electrochemical conversion of CO_2 to useful chemicals: current status, remaining challenges, and future opportunities," *Current Opinion in Chemical Engineering*, vol. 2, no. 2, pp. 191–199, 2013.

[7] J. Qiao, Y. Liu, F. Hong, and J. Zhang, "A review of catalysts for the electroreduction of carbon dioxide to produce low-carbon fuels," *Chemical Society Reviews*, vol. 43, no. 2, pp. 631–675, 2014.

[8] A. J. Martín, G. O. Larrazábal, and J. Pérez-Ramírez, "Towards sustainable fuels and chemicals through the electrochemical reduction of CO_2: lessons from water electrolysis," *Green Chemistry*, vol. 17, no. 12, pp. 5114–5130, 2015.

[9] R. Küngas, "Review—electrochemical CO_2 reduction for CO production: comparison of low- and high-temperature electrolysis technologies," *Journal of the Electrochemical Society*, vol. 167, no. 4, article 044508, 2020.

[10] J. T. Feaster, C. Shi, E. R. Cave et al., "Understanding selectivity for the electrochemical reduction of carbon dioxide to formic acid and carbon monoxide on metal electrodes," *ACS Catalysis*, vol. 7, no. 7, pp. 4822–4827, 2017.

[11] J. Rosen, G. S. Hutchings, Q. Lu, R. V. Forest, A. Moore, and F. Jiao, "Electrodeposited Zn dendrites with enhanced CO selectivity for electrocatalytic CO_2 reduction," *ACS Catalysis*, vol. 5, no. 8, pp. 4586–4591, 2015.

[12] F. Quan, D. Zhong, H. Song, F. Jia, and L. Zhang, "A highly efficient zinc catalyst for selective electroreduction of carbon dioxide in aqueous NaCl solution," *Journal of Materials Chemistry A*, vol. 3, no. 32, pp. 16409–16413, 2015.

[13] D. H. Won, H. Shin, J. Koh et al., "Highly efficient, selective, and stable CO_2 electroreduction on a hexagonal Zn catalyst," *Angewandte Chemie, International Edition*, vol. 55, no. 32, pp. 9297–9300, 2016.

[14] M. P. L. Kang, M. J. Kolb, F. Calle-Vallejo, and B. S. Yeo, "The role of undercoordinated sites on zinc electrodes for CO_2 reduction to CO," *Advanced Functional Materials*, vol. 32, no. 23, article 2111597, 2022.

[15] Z. Chen, K. Mou, S. Yao, and L. Liu, "Zinc-coordinated nitrogen-codoped graphene as an efficient catalyst for selective electrochemical reduction of CO_2 to CO," *ChemSusChem*, vol. 11, no. 17, pp. 2944–2952, 2018.

[16] Y. Hori, A. Murata, K. Kikuchi, and S. Suzuki, "Electrochemical reduction of carbon dioxides to carbon monoxide at a gold electrode in aqueous potassium hydrogen carbonate," *Journal of the Chemical Society, Chemical Communications*, no. 10, pp. 728-729, 1987.

[17] C. Chen, B. Zhang, J. Zhong, and Z. Cheng, "Selective electrochemical CO_2 reduction over highly porous gold films," *Journal of Materials Chemistry A*, vol. 5, no. 41, pp. 21955–21964, 2017.

[18] Y. S. Ham, S. Choe, M. J. Kim, T. Lim, S.-K. Kim, and J. J. Kim, "Electrodeposited ag catalysts for the electrochemical reduction of CO_2 to CO," *Applied Catalysis B: Environmental*, vol. 208, pp. 35–43, 2017.

[19] B. Kumar, J. P. Brian, V. Atla et al., "New trends in the development of heterogeneous catalysts for electrochemical CO_2 reduction," *Catalysis Today*, vol. 270, pp. 19–30, 2016.

[20] N. Zhang, X. Zhang, L. Tao et al., "Silver single-atom catalyst for efficient electrochemical CO_2 reduction synthesized from thermal transformation and surface reconstruction," *Angewandte Chemie International Edition*, vol. 60, no. 11, pp. 6170–6176, 2021.

[21] P. Delahay, M. Pourbaix, and P. Van Rysselberghe, "Potential-pH diagram of zinc and its applications to the study of zinc corrosion," *Journal of the Electrochemical Society*, vol. 98, no. 3, p. 101, 1951.

[22] W. Luo, Q. Zhang, J. Zhang, E. Moioli, K. Zhao, and A. Züttel, "Electrochemical reconstruction of ZnO for selective reduction of CO_2 to CO," *Applied Catalysis B: Environmental*, vol. 273, article 119060, 2020.

[23] T. Burdyny and W. A. Smith, "CO_2 reduction on gas-diffusion electrodes and why catalytic performance must be assessed at commercially-relevant conditions," *Energy & Environmental Science*, vol. 12, no. 5, pp. 1442–1453, 2019.

[24] D. M. Weekes, D. A. Salvatore, A. Reyes, A. Huang, and C. P. Berlinguette, "Electrolytic CO_2 reduction in a flow cell," *Accounts of Chemical Research*, vol. 51, no. 4, pp. 910–918, 2018.

[25] S. Hernandez-Aldave and E. Andreoli, "Fundamentals of gas diffusion electrodes and electrolysers for carbon dioxide utilisation: challenges and opportunities," *Catalysts*, vol. 10, no. 6, p. 713, 2020.

[26] H. Rabiee, L. Ge, X. Zhang, S. Hu, M. Li, and Z. Yuan, "Gas diffusion electrodes (GDEs) for electrochemical reduction of carbon dioxide, carbon monoxide, and dinitrogen to value-added products: a review," *Energy & Environmental Science*, vol. 14, no. 4, pp. 1959–2008, 2021.

[27] G. H. Han, J. Kim, S. Jang et al., "Catalyst for gaseous CO_2 electrolyzer," *Advancement of Science*, vol. 9, article 2104908, 2022.

[28] U. O. Nwabara, E. R. Cofell, S. Verma, E. Negro, and P. J. A. Kenis, "Durable cathodes and electrolyzers for the efficient aqueous electrochemical reduction of CO_2," *ChemSusChem*, vol. 13, no. 5, pp. 855–875, 2020.

[29] L. Ge, H. Rabiee, M. Li et al., "Electrochemical CO_2 reduction in membrane-electrode assemblies," *Chem*, vol. 8, no. 3, pp. 663–692, 2022.

[30] S. Garg, C. A. Rodriguez, T. E. Rufford, J. R. Varcoe, and B. Seger, "How membrane characteristics influence the performance of CO_2 and CO electrolysis," *Energy & Environmental Science*, vol. 15, no. 11, pp. 4440–4469, 2022.

[31] J. Kim, W. Guo, H. Kim, S. Choe, S. Y. Kim, and S. H. Ahn, "Gaseous CO_2 electrolysis: progress, challenges, and prospects," *ACS Sustainable Chemistry & Engineering*, vol. 10, no. 43, pp. 14092–14111, 2022.

[32] C. Kim, J. C. Bui, X. Luo et al., "Tailored catalyst microenvironments for CO_2 electroreduction to multicarbon products on copper using bilayer ionomer coatings," *Nature Energy*, vol. 6, no. 11, pp. 1026–1034, 2021.

[33] A. Patru, T. Binninger, B. Pribyl, and T. J. Schmidt, "Design principles of bipolar electrochemical co-electrolysis cells for efficient reduction of carbon dioxide from gas phase at low temperature," *Journal of The Electrochemical Society*, vol. 166, no. 2, pp. F34–F43, 2019.

[34] Y. Zhao, X. Zu, R. Chen et al., "Industrial-current-density CO_2-to-C_{2+} electroreduction by anti-swelling anion-exchange ionomer-modified oxide-derived cu nanosheets," *Journal of the American Chemical Society*, vol. 144, no. 23, pp. 10446–10454, 2022.

[35] R. Jervis, N. Mansor, A. J. Sobrido et al., "The importance of using alkaline ionomer binders for screening electrocatalysts in alkaline electrolyte," *Journal of The Electrochemical Society*, vol. 164, no. 14, pp. F1551–F1555, 2017.

[36] M. Chang, W. Ren, W. Ni, S. Lee, and X. Hu, "Ionomers modify the selectivity of cu-catalyzed electrochemical CO_2 Reduction," *ChemSusChem*, vol. 16, no. 5, article e202201687, 2023.

[37] J. Kim, H. Kim, G. H. Han, and S. H. Ahn, "Solution-phase-reconstructed Zn-based nanowire electrocatalysts for electrochemical reduction of carbon dioxide to carbon monoxide," *International Journal of Energy Research*, vol. 45, no. 5, pp. 7987–7997, 2021.

[38] B. Qin, Y. Li, H. Fu et al., "Electrochemical reduction of CO_2 into tunable syngas production by regulating the crystal facets of earth-abundant Zn catalyst," *ACS Applied Materials & Interfaces*, vol. 10, no. 24, pp. 20530–20539, 2018.

[39] S. Kumar, S. Chatterjee, K. K. Chattopadhyay, and A. K. Ghosh, "Sol–gel-derived ZnO:Mn nanocrystals: study of structural, Raman, and optical properties," *Journal of Physical Chemistry C*, vol. 116, no. 31, pp. 16700–16708, 2012.

[40] M. Wang, L. Jiang, E. J. Kim, and S. H. Hahn, "Electronic structure and optical properties of $Zn(OH)_2$: LDA+U calculations and intense yellow luminescence," *RSC Advances*, vol. 5, no. 106, pp. 87496–87503, 2015.

[41] D. L. T. Nguyen, M. S. Jee, D. H. Won et al., "Selective CO_2 reduction on zinc electrocatalyst: the effect of zinc oxidation state induced by pretreatment environment," *ACS Sustainable Chemistry & Engineering*, vol. 5, no. 12, pp. 11377–11386, 2017.

[42] I. Stamatelos, C.-T. Dinh, W. Lehnert, and M. Shviro, "Zn-based catalysts for selective and stable electrochemical CO_2 reduction at high current densities," *ACS Applied Energy Materials*, vol. 5, no. 11, pp. 13928–13938, 2022.

[43] L.-C. Weng, A. T. Bell, and A. Z. Weber, "Towards membrane-electrode assembly systems for CO_2 reduction: a modeling study," *Energy & Environmental Science*, vol. 12, no. 6, pp. 1950–1968, 2019.

[44] R. B. Kutz, Q. Chen, H. Yang, S. D. Sajjad, Z. Liu, and I. R. Masel, "Sustainion imidazolium-functionalized polymers for carbon dioxide electrolysis," *Energy Technology*, vol. 5, no. 6, pp. 929–936, 2017.

[45] Z. Liu, H. Yang, R. Kutz, and R. I. Masel, "CO_2 electrolysis to CO and O_2 at high selectivity, stability and efficiency using Sustainion membranes," *Journal of the Electrochemical Society*, vol. 165, no. 15, pp. J3371–J3377, 2018.